Why do the global warming responses of land-surface models and climatic dryness metrics disagree?

Jacob Scheff[1], **Sloan Coats**[2], **and Marysa Laguë**[3]

[1]Department of Geography and Earth Sciences, University of North Carolina, Charlotte, NC, USA
[2]Department of Earth Sciences, University of Hawai'i, Honolulu, HI, USA
[3]Coldwater Laboratory and Center for Hydrology, University of Saskatchewan, Canmore, AB, Canada

Key Points:

- CLM5 runoff ratio and soil moisture responses to climate change closely follow the aridity index and PDSI in a simplified simulation
- Runoff ratio increases much more than aridity index in full simulations primarily due to changes in the temporal pattern of precipitation
- Soil moisture increases more than PDSI in full simulations primarily due to CO2 and vapor pressure deficit effects on plant physiology

Corresponding author: Jacob Scheff, jscheff@uncc.edu

Abstract

Earth System Models' complex land components simulate a patchwork of increases and decreases in surface water availability when driven by projected future climate changes. Yet, commonly-used simple theories for surface water availability, such as the Aridity Index (P/E0) and Palmer Drought Severity Index (PDSI), obtain severe, globally dominant drying when driven by those same climate changes, leading to disagreement among published studies. In this work, we use a common modeling framework to show that ESM simulated runoff-ratio and soil-moisture responses become much more consistent with the P/E0 and PDSI responses when several previously known factors that the latter do not account for are cut out of the simulations. This reconciles the disagreement and makes the full ESM responses more understandable. For ESM runoff ratio, the most important factor causing the more positive global response compared to P/E0 is the concentration of precipitation in time with greenhouse warming. For ESM soil moisture, the most important factor causing the more positive global response compared to PDSI is the effect of increasing carbon dioxide on plant physiology, which also drives most of the spatial variation in the runoff ratio enhancement. The effect of increasing vapor-pressure deficit on plant physiology is a key secondary factor for both. Future work will assess the utility of both the ESMs and the simple indices for understanding observed, historical trends.

Plain Language Summary

Rivers and groundwater provide almost all water used by humans, and soil moisture is critical for vegetation and crops worldwide. Supercomputer model simulations of rivers, groundwater and soil moisture under future global warming routinely project that some world regions will experience increases in the availability of these resources, while others will experience decreases. Yet the simple formulas that scientists have traditionally relied on to measure climatic "drought" and "aridity" obtain large future decreases in water availability (drying) almost everywhere. This has led to confusion in prior studies and reports. In this study, we resolve this apparent paradox by pinpointing exactly why the supercomputer simulations are less pessimistic than the simple formulas. For rivers and groundwater, the most important reason is that precipitation gets "flashier" and more intense with global warming. For soil moisture, the most important reason is that increasing carbon dioxide allows vegetation to use less water, keeping more water in the soil. Both of these processes are included in the computer models, but not in the simple formulas. This new understanding gives us greater confidence that the computer models are behaving reasonably.

1 Introduction

Fresh water at Earth's surface is critical for all terrestrial life, including human life. Therefore, reports of anthropogenic climate change effects on terrestrial water scarcity (as cited in, e.g., Douville et al. (2021) and Seneviratne et al. (2021)) are of fundamental interest. At the global scale, such studies generally employ one of two common methodologies.

On one hand, the complex land-surface models embedded in Earth System Models (ESMs; Eyring et al., 2016) are used to perform explicit but difficult-to-parse simulations of the effects of climate and CO_2 changes on particular terrestrial water fluxes (e.g., runoff) or stocks (e.g., soil moisture). Recent studies using this approach include Berg and Sheffield (2018), Lemordant et al. (2018), and Cook et al. (2020).

On the other hand, simple, widely-used theories for general terrestrial water abundance based on precipitation (P) and potential evaporation (E_0), such as the aridity index (P/E_0; Transeau, 1905; Budyko & Miller, 1974), the Palmer Drought Severity Index (PDSI; Palmer, 1965), and the Standardized Precipitation-Evapotranspiration In-

dex (SPEI; Vicente-Serrano et al., 2010), are used to assess projected global warming impacts on future water availability. Recent studies using this approach include Naumann et al. (2018), Dai et al. (2018), Wang et al. (2020), Vicente-Serrano et al. (2020), and Qi et al. (2022).

In recent years, however, it has become clear (Zhao & Dai, 2015; Roderick et al., 2015; Swann et al., 2016; Milly & Dunne, 2016, 2017; Scheff et al., 2017; Scheff, 2018; Berg & Sheffield, 2018; Greve et al., 2019; Y. Yang et al., 2019, 2020) that these two approaches yield fundamentally conflicting results at the global scale. ESM land-surface outputs, especially those of runoff, precipitation-minus-evapotranspiration, and root-zone soil moisture, generally depict a regional patchwork of increases and decreases in water availability. Yet P/E_0, PDSI, and SPEI, when driven by the same ESMs' climate outputs, usually obtain near-global drying equatorward of $\approx 55°$ (with just a few regional exceptions). These apparent contradictions, which we have termed "dryness index-impact gaps" (Scheff et al., 2021), call into question the reliability of both the ESM land models and the simple theories. They are often apparent in Tables 11.3-11.21 of Seneviratne et al. (2021), where they lead to difficulty in assessing the sign of climate change effects on drought.

Many of the studies cited above argue that the index-impact gaps arise primarily because the ESM land models account for the closure of leaf stomates by elevated CO_2, counteracting the warming-driven evapotranspiration increase that drives the global drying response in the simple theories. However, we have found in prior work that though this effect largely explains the gap between ESM vegetation responses and the simple theories, it does not explain many of the gaps between ESM *hydrologic* responses and the simple theories (Scheff et al., 2021). Even in special multi-ESM experiments in which CO_2-plant effects are completely turned off (Jones et al., 2016), the runoff ratio still responds much more positively than P/E_0, PDSI or SPEI to global warming, despite the theoretical idea that P/E_0 is the main control on the runoff ratio (Budyko & Miller, 1974; Gentine et al., 2012). Similarly, in those experiments, the SPEI still responds much more negatively than root-zone soil moisture (Scheff et al., 2021), despite its goal of quantifying the effect of climate change on water availability (Vicente-Serrano et al., 2010).

Therefore, in this study, we use the Community Land Model (CLM; Lawrence et al., 2019), a widely-adopted land ESM, to test several alternative reasons for the hydrologic index-impact gaps other than CO_2-plant effects. These include closure of leaf stomates by elevated vapor-pressure deficits (Novick et al., 2016; Massmann et al., 2019), concentration of precipitation into shorter, more intense events with warming (Pendergrass & Hartmann, 2014; Zhao & Dai, 2015; H. Yang et al., 2018; Mankin et al., 2019), and concentration of precipitation into the existing wet season (Chou et al., 2013; R. J. Allen & Anderson, 2018). All of these have been previously hypothesized to alter surface water availability. However, they have largely been untested in a modeling framework, though H. Yang et al. (2018) did show a key role for the concentration of P using a statistical method.

2 Methods

2.1 Model and experiments

To perform these experiments, we use CLM5.0, which is the edition of the CLM used in the Community Earth System Model version 2 (CESM2; Danabasoglu et al., 2020) that participated in the Coupled Model Intercomparison Project phase 6 (CMIP6; Eyring et al., 2016). We run CLM5.0 on the Cheyenne system (Computational and Information Systems Laboratory, 2019). CLM5.0's innovations (Lawrence et al., 2019) relative to CLM4.5 include updated hydrologic and snow parameterizations with spatially varying soil depth, a plant-hydraulic parameterization to more realistically account for veg-

Table 1. CLM5.0 experiments in this study.

Present (1965-2014)	Future (2051-2100)	Difference
default	default	"default"
CLM5.0 CO_2 = 370 ppm	CLM5.0 CO_2 = 370 ppm	"fixedCO2"
Medlyn VPD = 1.5 kPa	Medlyn VPD = 1.5 kPa	"medlynconst"
default	pseudofuture	"noflash"
default	pseudofuture2	"noflashnoseas"
370 ppm and 1.5 kPa	pseudofuture2 with 370 ppm and 1.5 kPa	"allelim"

etation water stress, and a new stomatal scheme that uses the model of Medlyn et al. (2011).

We drive CLM5.0 using stored CESM2 atmospheric coupler history from the CMIP6 historical and "SSP5-8.5" (high-emission future) experiments, rather than running coupled CESM2 simulations. This saves computational time, simplifies the problem by focusing on the hydrologic response to atmospheric change, and, critically, allows us to test hypotheses by manipulating the driving data more easily (see below). However, this decision also disables land-atmosphere feedback, which may drive a key part of these responses (e.g., Berg et al., 2016; Zhou et al., 2021). Therefore, future work should expand these questions to fully-coupled simulations so as to quantify the feedback-driven component.

For our default present experiment, we drive CLM5.0 using years 1965-2014 of the `b.e21.BHIST.f09_g17.CMIP6-historical.011` run's coupler history, discarding 1965-1984 for spinup and only analyzing 1985-2014. For our default future experiment, we drive CLM5.0 using years 2051-2100 of the `b.e21.BSSP585cmip6.f09_g17.CMIP6-SSP5-8.5.102` run's coupler history, discarding 2051-2070 for spinup and only analyzing 2071-2100. We set CLM5.0 to read the diagnostic CO_2 from the coupler history, so that these runs "see" the CO_2 changes in addition to the climate changes. The difference between these future and present outputs is termed "default". The driving files are all available in the National Center for Atmospheric Research's Campaign Storage system under `/glade/campaign/collections/cmip/CMIP6/cpl_hist/`, and include daily ("1d"), 3-hourly ("3h"), and two types of hourly ("1h" and "1hi") files.

We then perform a series of alternative runs, listed in Table 1, to test the role of each proposed factor in creating the index-impact gaps. Again, a couple of these factors (CO_2-plant effects and P temporal concentration) have been tested with modeling and/or statistical techniques in prior studies, but they have never been tested together or compared using a common modeling framework.

To isolate the role of CO_2-plant effects as in Scheff et al. (2021), we run present and future experiments in which CLM5.0's CO_2 is fixed to 370 ppm (a representative value for 1985-2014) rather than read in diagnostically. The difference between these is termed "fixedCO2". To isolate the role of VPD-stomatal effects as in Novick et al. (2016), we run present and future experiments in which the VPD input to the Medlyn stomatal code is fixed to a constant 1.5 kPa. The difference between these is termed "medlynconst". Of course, these values would never be fixed in nature; our goal in fixing them is to deliberately *cut out* or *disable* the process in question (e.g., Kim et al., 2011), so that simulations with and without the process can be compared in section 3.

To isolate the role of the concentration of precipitation in time with warming as in Pendergrass and Hartmann (2014) and H. Yang et al. (2018), we create a "pseudo-SSP5-8.5" driving dataset with the climate properties of SSP5-8.5 but the temporal weather

characteristics of the historical dataset. First, for each driving variable, day of year, and (for sub-daily variables) time of day, historical (1985-2014) and SSP5-8.5 (2071-2100) climatology fields are computed. At each time of day (so as not to smooth across the diurnal cycle), these climatologies are further smoothed with a 31-day running mean. They are then divided (subtracted, in the case of temperature and pressure) to form a seasonally and diurnally varying perturbation field for each variable. This perturbation field is finally multiplied by (added to) all 50 years of the time-varying historical driving data to create the pseudo-SSP5-8.5 data, which then drives our "pseudofuture" run. The difference between the pseudofuture and the default present is then termed "noflash" (the effect of global warming and CO_2 increase without the "flashier" precipitation).

The reason we create and use this pseudo-SSP5-8.5 data for *every* driving variable, is that setting precipitation *alone* to pseudo-SSP5-8.5 (i.e., historical weather history) while keeping other variables SSP5-8.5 (i.e., future weather history) would destroy the short-term correlations between precipitation and other variables, introducing an additional change. However, at the rare times and locations where a variable's perturbation factor is greater than 5, the original SSP5-8.5 data for that variable is used to avoid unrealistic values.

Also, certain closely-related variables from the coupler are immediately combined by CLM5.0 to create "macro-variables," which it then uses in place of the original variables. Specifically, CLM5.0 adds the convective rain, large-scale rain, convective snow, and large-scale snow fluxes from the coupler before imposing its own partitioning, so we also add these four fluxes before computing the climatology, and we apply the resulting perturbation to each flux. This avoids large artificial total-precipitation changes caused by, e.g., snow changing to rain. Similarly, CLM5.0 adds the wet and dry deposition rates for each aerosol species that has wet and dry deposition, so we do the same. Finally, CLM5.0's surface turbulence scheme only depends on the wind speed and not the u and v components, so we convert the u and v components into wind speed before computing our wind climatology and perturbation, which we then apply to both u and v.

To isolate the role of changing precipitation seasonality as in Chou et al. (2013), we also run a "pseudofuture2" experiment that is identical to pseudofuture except that the above precipitation perturbation is based only on the *annual-mean* climatologies at each location and time of day. Our time-varying pseudofuture2 precipitation thus has the annual-mean climatology of SSP5-8.5, but the weather *and seasonality* of the historical. Since in this case there is no danger of ruining the synoptic-scale correlations, only the precipitation is altered in this way, for simplicity. The difference between the pseudofuture2 and the default present is termed "noflashnoseas". Again, our purpose here is to compare "noflash" and "noflashnoseas" to the default simulation, so as to quantify the contributions of weather and P seasonality changes to the default simulation.

Last, we run a pair of experiments like the present and pseudofuture2 runs, but with CO_2 fixed to 370 ppm and the Medlyn code's VPD fixed to 1.5 kPa (for both). These test the effects of making all of the above simplifications at once, and allow us to check for any nonlinear interactions between them. The difference between this pair is termed "allelim" (i.e., the effect of climate change with the complicating factors all eliminated).

2.2 Deriving monthly hydroclimate variables

Since CLM5.0 outputs its key driving fluxes and near-surface meteorological fields in addition to the usual land-surface output, we read in or compute all of our required monthly land *and atmospheric* variables from the CLM5.0 output, for simplicity.

We compute monthly precipitation P as the sum of `RAIN_FROM_ATM` and `SNOW_FROM_ATM`, and read in evapotranspiration E from `QFLUX_EVAP_TOT` and total runoff Q from `QRUNOFF`. With these definitions, each run's annual-mean climatology of Q is essentially identical

to that of $P - E$ (not shown), so CLM5.0 is defining Q correctly and conserving water. We compute raw monthly layer-by-layer soil moisture (in mm) as `SOILLIQ` plus `SOILICE`, and then define surface soil moisture SM_s to be the sum of the first 3 layers (12 cm) of soil moisture, and deep or root-zone soil moisture SM_d to be the sum of the first 11 layers ($\approx$ 2 m) of soil moisture.

We then compute monthly FAO-56 (Food and Agriculture Organization; R. G. Allen et al., 1998) Penman-Monteith potential evapotranspiration E_0 and effective relative humidity RH, as in Scheff et al. (2021). We use `EFLX_LH_TOT` (latent heat flux) plus `FSH` (sensible heat flux) for the available energy $(\mathrm{LH} + \mathrm{SH}) = R_n - G$. We use `TSA` for the air temperature, `PBOT` for the air pressure, `Q2M` for the air humidity, and `U10` for the wind speed. Using the monthly P and E_0 series, we compute the PDSI and 12-month SPEI each month, also as in Scheff et al. (2021). For each experiment, the PDSI and SPEI reference period is years 1985-2014 of that experiment (Table 1).

2.3 Annual series and statistics

Assessing the statistical significance of any present-future changes using monthly series would be difficult, because most of these variables have strong annual cycles of both mean and variance, and many have significant month-to-month memory. Therefore, we carefully construct annual series from each 50-year run's monthly series, as follows.

First, at each gridpoint, for each of P, Q, SM_s, SM_d, RH, PDSI, and (LH+SH), we define that variable's "water year" (for LH+SH, "energy year") to end on the calendar month with the least interannual variance of that variable. For example, if at some gridpoint July has the least interannual variance of SM_d out of all 12 calendar months, the SM_d water year at that gridpoint is defined to begin in August and end in July. This ensures that most of the interannual differences do not straddle consecutive years. We then average each aforementioned variable's monthly series over its respective 49 water years to obtain 49 annual values (though we only analyze the last 29 below, for spinup reasons as stated in section 2.1). Where the water year is January through December (yielding 50 water years), we average over the last 49.

Other key variables' annual values are computed as follows. For P/E_0, we average E_0 over the P water years, and then divide the annual-mean P and annual-mean E_0 series to form annual P/E_0 series. For 12-month SPEI, we simply choose the values that correspond to the P water years, and discard the rest, forming annual SPEI series. For evaporative fraction EF, we average LH over the (LH+SH) "energy years", and then divide the annual LH and annual (LH+SH) series to form annual series of EF. Similarly, for runoff ratio Q/P, we average P over the Q water years, and divide the Q series by the resulting P series to obtain annual Q/P series. (This is not perfect since P that falls in one water year can become Q in a subsequent one, but it still seems reasonable to assume that most of a water year's Q comes from P that fell during that time.)

To quantify interannual variability, we take the standard deviation of each of the above annual series over the last 29 water years (1985-2014) of each present run. To quantify the mean hydroclimate of each epoch, we similarly take the mean of each of the above annual series over the last 29 water years of each present (1985-2014) and (pseudo)future (2071-2100) run, for most variables. However, we define mean P/E_0 as mean P over mean E_0, mean EF as mean LH over mean (LH+SH), and mean Q/P as mean Q over mean P, consistent with prior literature (e.g., Budyko & Miller, 1974).

Finally, we subtract the future and present means for each pair of runs in Table 1, and divide by the present interannual variability, to obtain *standardized changes* in each variable for each experiment. We also compute differences in standardized changes between index and impact variables, so as to quantify the qualitative index-impact gaps discussed in section 1. For example, wherever variable A significantly declines from present

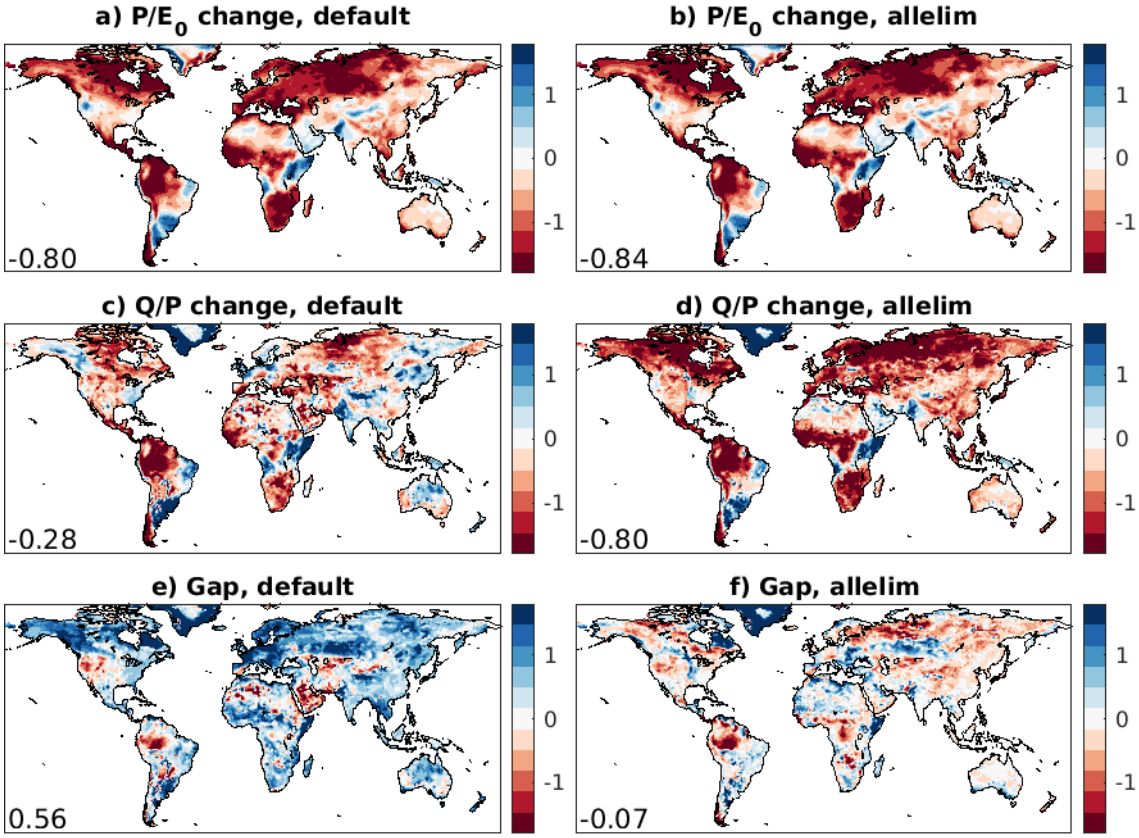

Figure 1. CLM5.0 standardized changes from 1985-2014 (historical) to 2071-2100 (SSP5-8.5) in annual aridity index P/E_0 and runoff ratio Q/P, and the difference or gap between those changes. Left: default experiment. Right: "allelim" experiment, in which CO_2-plant effects, vapor-pressure-deficit effects on leaf physiology, and changes to the temporal pattern of precipitation are all disabled. Numbers at lower left of each panel are medians over ice-free land.

to future but variable B only insignificantly declines from present to future, variable B's standardized change is less negative than variable A's standardized change, so their difference (gap) is positive.

3 Results

3.1 Aridity index vs. runoff ratio

We first address the long-standing gap between simulated P/E_0 and Q/P responses to climate change, which is surprising given that P/E_0 is theorized and observed to be the main control on Q/P worldwide (Budyko & Miller, 1974; Gentine et al., 2012).

Figure 1 (left) shows that in the default CLM5.0 experiment, Q/P indeed decreases less extensively and significantly than one would think from the map of P/E_0 change. The standardized-change gap between the two in Figure 1e is strongly positive (median +0.56), with just a few regional exceptions. To be fair, we would not expect a P/E_0 change to cause a Q/P change of similar strength everywhere, since Q/P saturates at 0 in extremely dry regions and at 1 in extremely wet regions; but the positive gaps in Figure 1e extend far beyond such regions.

In any case, Figure 1 (right) shows that in the "allelim" experiment in which CO_2-plant effects, VPD-stomatal effects, and P temporal-pattern changes are eliminated, the CLM5.0-simulated Q/P change becomes much more negative, resembling the driving P/E_0 change quite closely. The gap becomes a mottled mix of positive and negative (median -0.07). Thus, the strong positivity of the gap in the default simulation (left) must stem from some combination of the above eliminated factors, rather than an inherent problem with P/E_0 as a runoff-ratio predictor.

Figure 2 explores what this combination could be, by plotting differences in the above Q/P - P/E_0 response gap between the default simulation and the various simplified simulations in Table 1. To be clear, these differences are almost entirely made up of differences in the Q/P response (Figure 1c-d), rather than the P/E_0 response which is largely set by the driving data (Figure 1a-b).

Figure 2a shows that the difference between the default and "allelim" gaps from Figure 1e-f (i.e., the effect on Q/P or on the Q/P - P/E_0 gap of all four targeted processes combined) is indeed large and positive, with a median of +0.57. A modest (median +0.09) but persistently positive portion of this difference comes from the closure of leaf stomates by elevated VPD (Novick et al., 2016) in the Medlyn parameterization, as shown in Figure 2b. The effect of CO_2-plant interactions in Figure 2c is much larger in absolute value and is clearly the main driver of the *spatial pattern* of the full difference. However, it is almost as likely to be negative (i.e., *reduce* Q/P) as positive, particularly in middle to low latitudes, so its median (+0.13) is only slightly more positive than that of the VPD effect. This agrees with the finding of Mankin et al. (2018, 2019) that leaf growth more than cancels the positive hydrologic effect of CO_2-driven stomatal closure over large regions in CESM1 and CMIP5.

In contrast, the effect of changes in the short-term temporal pattern of P on the Q/P response in Figure 2d is both moderately strong, and almost entirely positive, making its median (+0.22) quite a bit more positive than that of the CO_2 effect. We take this to reflect the concentration of P into shorter, more intense bursts (e.g. Pendergrass & Hartmann, 2014; H. Yang et al., 2018) that is likely widespread in the default experiment, but by design absent in the "noflash" experiment. The effect of P seasonality change in Figure 2e is mostly weak globally (median +0.05), but is strongly positive in mid-latitude Eurasia. This is precisely where models tend to project winter P to increase but summer P to decline (e.g., figure 4.24 in Lee et al., 2021), which would tend to enhance annual Q/P. The residual nonlinear term in Figure 2f is also mostly weak, though it does tend to be negative (median -0.06), implying that the whole is slightly less than the sum of the parts.

Figure 2g complements the global medians by mapping which effect is most positive at each gridpoint, i.e., which effect is the most important local contributor to the global tendency of the Q/P response to be more positive than the $P/E0$ response. Due to its large absolute values, the CO_2 effect (Figure 2c) dominates almost wherever it is positive: much of the high latitudes, the Tibetan Plateau, and parts of the low latitudes. However, over much of tropical and subtropical South America, Africa, South and Southwest Asia, and Australia, the concentration of P into shorter events (Figure 2d) is actually the most Q/P-enhancing effect, consistent with its more positive median. Furthermore, P seasonality change (Figure 2e) is the most Q/P-enhancing effect throughout its mid-latitude Eurasian zone of strength.

Thus, all four of the hypothesized processes seem to be at least somewhat important in explaining why CLM5.0's Q/P response is less negative than its driving P/E_0 response, with P temporal concentration most important in a global-median sense, but CO_2 and P-seasonality effects also very important regionally. To quantify which effects are the most important overall, Figure 3 plots cumulative distribution functions (CDFs)

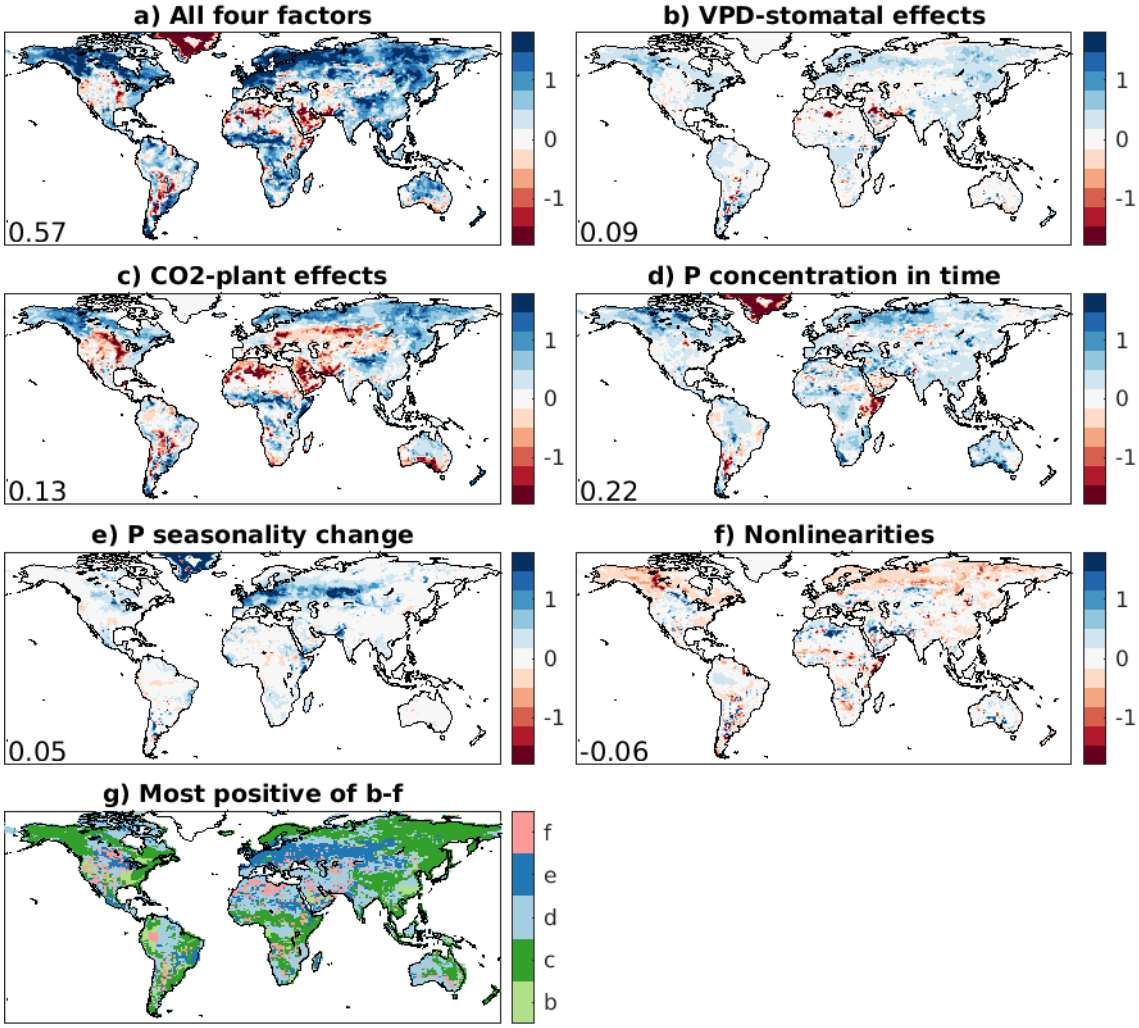

Figure 2. Q/P - P/E_0 standardized change gap differences between a) "default" minus "alle-lim" (i.e., the bottom panels of Figure 1), b) "default" minus "medlynconst", c) "default" minus "fixedCO2", d) "default" minus "noflash", e) "noflash" minus "noflashnoseas", and f) panel a minus the sum of panels b-e (see Table 1 for definitions). Each panel quantifies the contribution of its title to the Q/P - P/E_0 standardized change gap. Panels can also be directly interpreted as Q/P change differences, since P/E_0 change differences between experiments are very small. Numbers at lower left of each panel are medians over ice-free land. g) Which of panels b-f is most positive at each gridpoint.

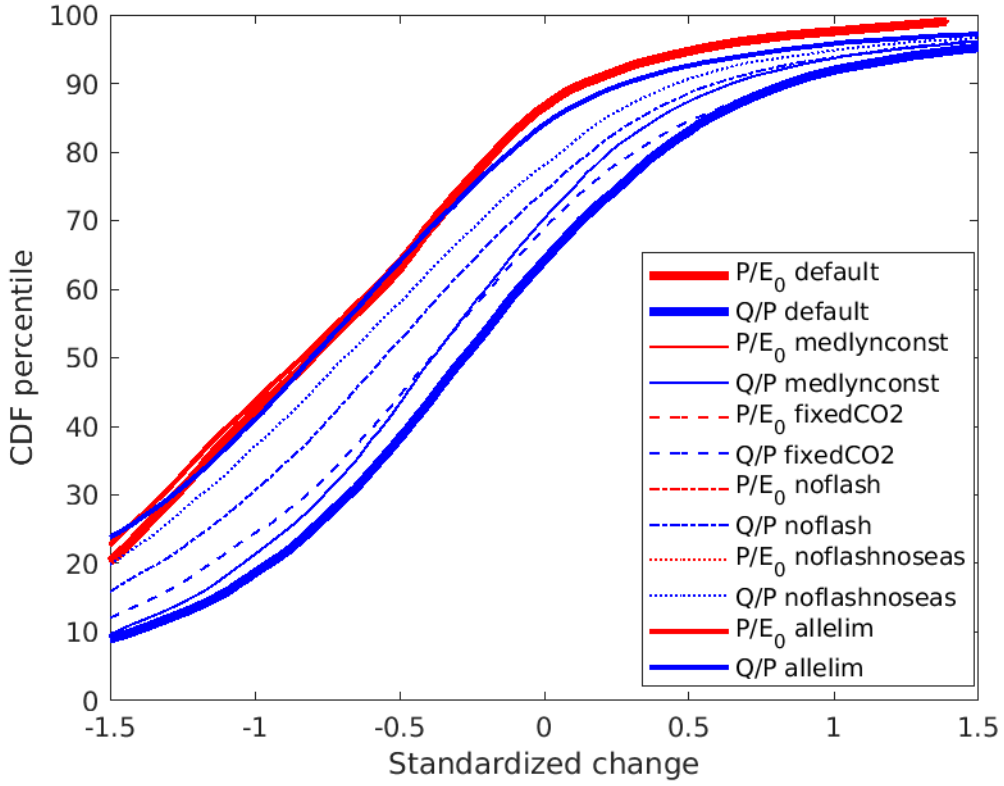

Figure 3. Cumulative distribution functions over ice-free land of the standardized responses of P/E_0 (red) and Q/P (blue) to SSP5-8.5 climate changes, for the default experiment (very thick solid curves), the simplifed "allelim" experiment (less-thick solid curves), and the intermediate experiments (the various thin curves) in Table 1. (The P/E_0 curves plot nearly on top of one another, since P/E_0 is largely set by the atmospheric driving data. Any P/E_0 differences stem from slight differences in the near-surface meteorological fields used to calculate E_0, which CLM computes based on the driving data, but which are not identical to it.)

of the P/E_0 and Q/P standardized change fields over ice-free land in each of the experiments in Table 1.

In the default experiment, the Q/P distribution (very thick blue) plots far to the right of the P/E_0 distribution (very thick red) in Figure 3, consistent with Figure 1e. However, in "allelim", the Q/P distribution (less-thick blue) plots almost directly on top of the P/E_0 distribution. This implies that the qualitative difference between the global responses of P/E_0 and Q/P almost completely vanishes when the above four processes are eliminated, consistent with Figure 1 (right).

Strikingly, just turning off changes in the short-term temporal pattern of P brings Q/P ~half or more of the way from the default distribution towards the allelim and P/E_0 distributions at most percentiles. This is shown by the dash-dotted blue "noflash" distribution in Figure 3. Further eliminating changes in the seasonality of P shifts the Q/P distribution yet closer to the P/E_0 distribution, as shown by the dotted "noflashnoseas" distribution. However, this shift from "noflash" to "noflashnoseas" is markedly smaller than the above shift from default to "noflash". Similarly, the Q/P distribution shifts from

default to "medlynconst" (VPD-leaf effects off) and from default to "fixedCO2" (CO_2-plant effects off) are each relatively small.

Thus, changes in the short-term temporal pattern of P, i.e., differences between the default and "noflash" distributions in Figure 3, appear to be the single largest contributor to the overall positive tendency of the gap between the default Q/P and P/E_0 responses, consistent with the spatial-median analysis in Figure 2 and with the regression-based results of H. Yang et al. (2018). This is likely because the effect on the gap is both consistently positive, and fairly large (Figure 2d). This process had been posited by studies such as Zhao and Dai (2015), Mankin et al. (2018), and Dai et al. (2018) to be an important reason why atmospheric dryness metrics like P/E_0 underestimate runoff responses in ESMs, but had not been verified by modeling experiments until now.

The relative similarity of the "fixedCO2" (dashed) and default Q/P distributions is also consistent with the finding of Scheff et al. (2021) that the Q/P - P/E_0 response gap only slightly narrows in CMIP runs with no CO_2-plant effects, contrary to the assumptions of many of the studies in section 1. In CLM5.0, this change is characterized by offsetting local positive and negative effects on Q/P (Figure 2c) and thus a relatively small net effect in Figure 3, despite its clear dominance of the spatial pattern. In fact, VPD-leaf effects and P seasonality changes each cause ∼equal or greater Q/P distribution shifts in Figure 3, reinforcing the idea that CO_2-plant effects are only one (small) cause of the positive global tendency.

3.2 PDSI vs. root-zone soil moisture

We next analyze the gap between the PDSI and SM_d responses, as in Berg and Sheffield (2018). PDSI is a common and well-used indicator of root-zone soil moisture, so qualitative differences between modeled PDSI and SM_d responses to climate change are also of theoretical and practical concern.

Figure 4 (left) shows that in the default warming experiment, CLM5.0 SM_d (median response -0.29) indeed declines less significantly and systematically than does PDSI (median response -0.53). Areas of qualitative difference between Figures 4a and c include Australia, the African Sahel and Sahara, eastern Asia, parts of Europe and Central Asia, and interior northwestern North America. All of these areas are apparent on the gap plot (Figure 4e) as well, which is largely positive outside of the highest latitudes (median +0.35).

Analogously to Q/P above, in the "allelim" experiment SM_d declines much more strongly in several of the above regions (Figure 4d), giving a somewhat more "PDSI-like" impression of dominant drying. In fact, the median SM_d and PDSI responses become almost identical (-0.63 and -0.67). Likewise, the gap plot (Figure 4f) becomes more balanced between positive and negative, with a median of 0.00. However, the default-allelim differences are more subtle than those in Figure 1, and the local absolute values of the gap in allelim on Figure 4f remain quite large. Thus, it seems that the PDSI and CLM5.0 models of soil moisture disagree for many reasons beyond the four factors tested here.

However, some combination of the four factors must still be responsible for much of the positive *tendency* of the SM_d - PDSI gap in Figure 4e, since again there is considerably less of a positive tendency in Figure 4f. Figure 5 shows that the greatest apparent contributor to the difference between Figures 4e-f (Figure 5a) is the CO_2 effect on plants, which tends to increase SM_d (Figure 5c; median +0.39), more than accounting for the total gap. The VPD-leaf effect on SM_d (Figure 5b) is more consistently positive than the CO_2 effect, but weaker (median +0.15). The temporal-pattern effects (Figure 5d-e) tend to be negative, presumably because more temporally concentrated P leads to greater surface runoff but less infiltration (Eekhout et al., 2018). The nonlinear term (Figure 5f) also tends to be negative. Thus, the CO_2 effect is the most positive contributor at most gridpoints (Figure 5g), though the other terms are also locally important.

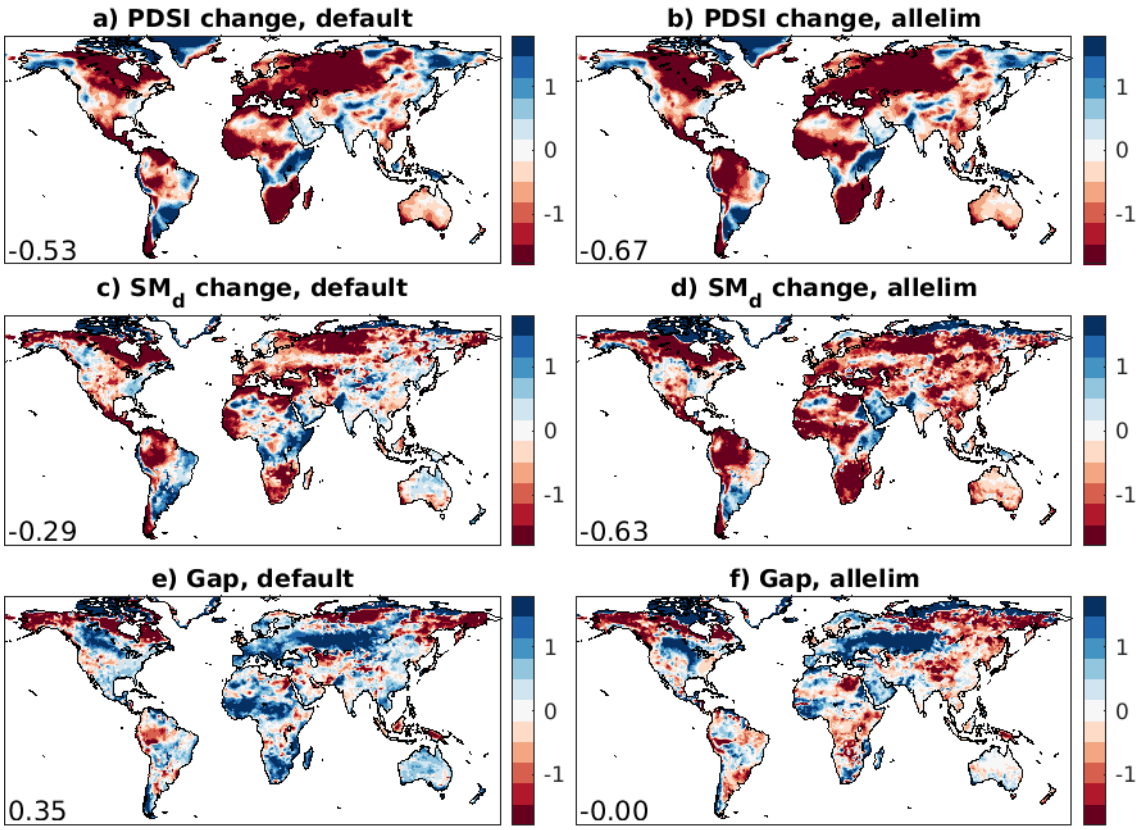

Figure 4. As Figure 1, but for Palmer Drought Severity Index PDSI and deep-layer soil moisture SM_d.

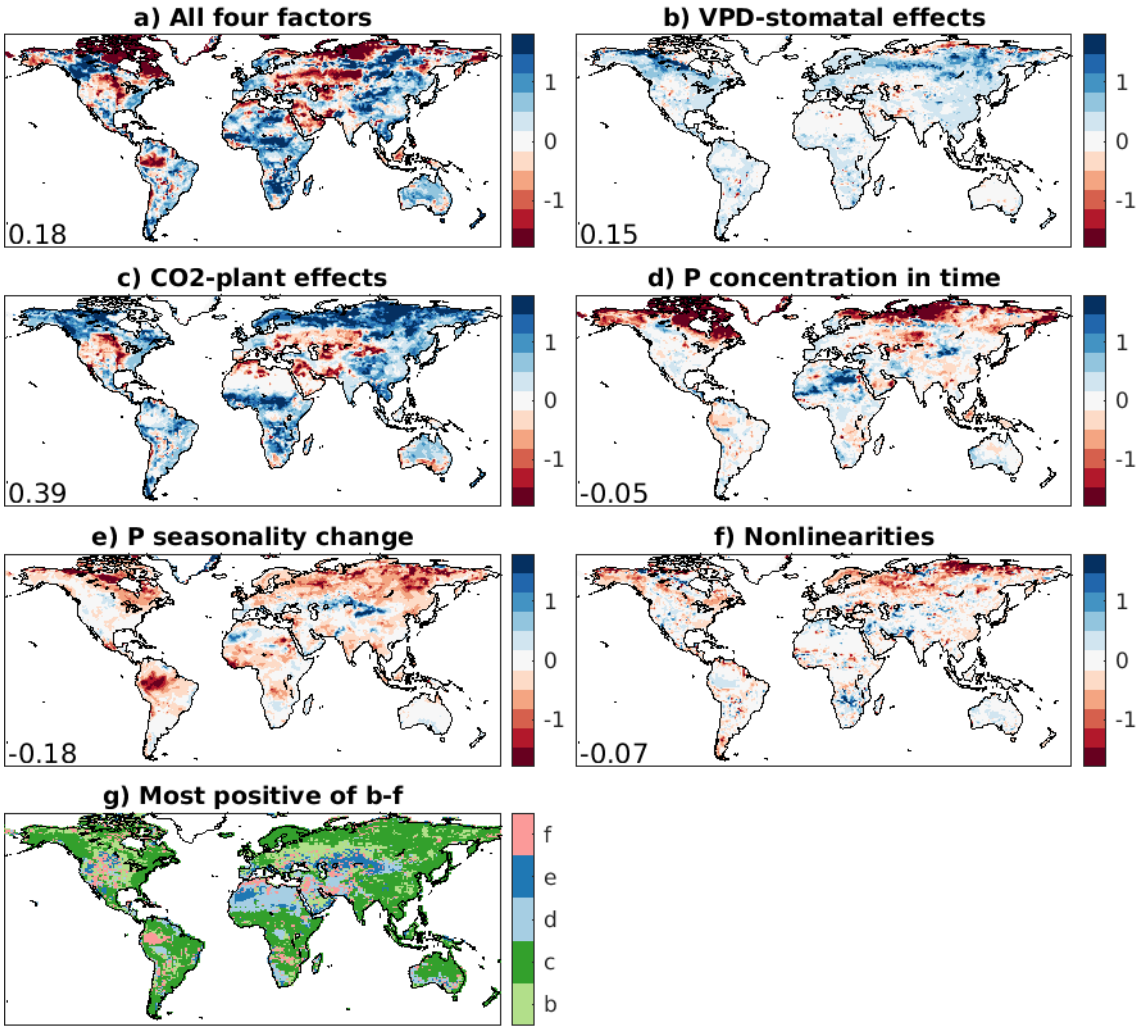

Figure 5. As Figure 2, but for the SM_d - PDSI gap.

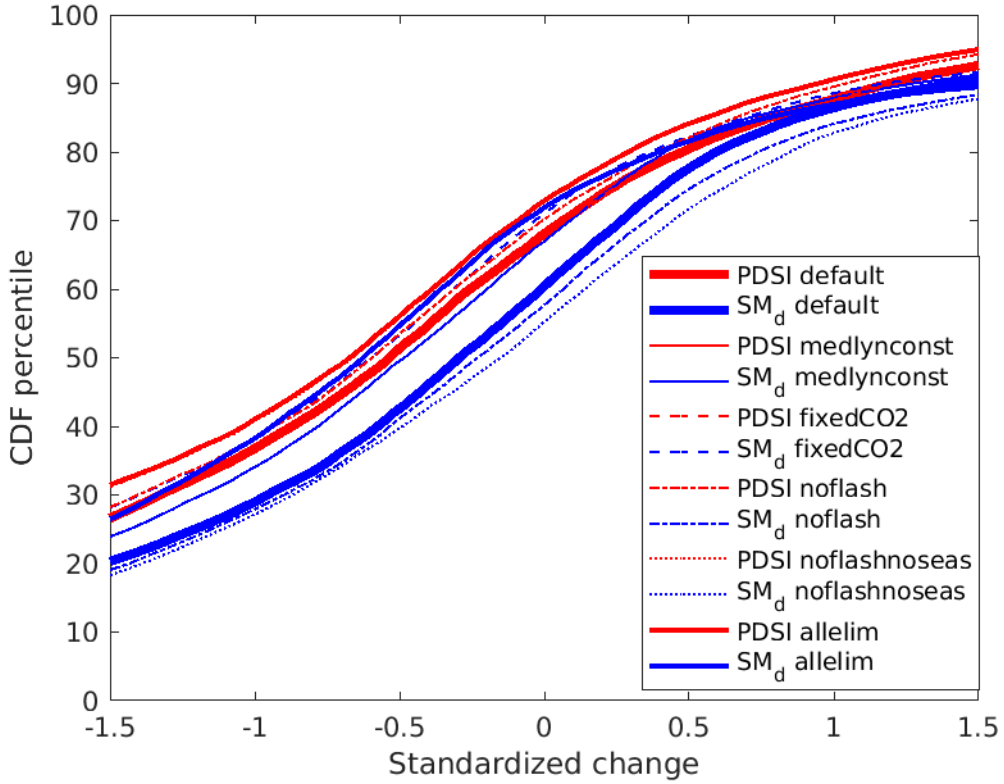

Figure 6. As Figure 3, but for PDSI (red) and SM_d (blue). The PDSI medlynconst and PDSI fixedCO2 curves plot on top of the PDSI default curve, and the PDSI noflashnoseas curve plots on top of the PDSI allelim curve.

The PDSI and SM_d standardized response distributions in Figure 6 confirm both the modest but real qualitative gap in the default simulation (very thick curves) and the closing of this gap in the allelim simulation (less-thick curves), particularly in the middle percentiles. Consistent with the discussion of Figure 5, eliminating CO_2-plant effects is more than sufficient to close the gap: the SM_d fixedCO2 curve actually plots to the *left* of the PDSI fixedCO2 curve, which is on top of the PDSI default curve. This corroborates the findings of Scheff et al. (2021) and Y. Yang et al. (2020) that the SM_d - PDSI gap in the full CMIP ensemble can largely be explained by CO_2-plant effects.

Surprisingly, the elimination of VPD-leaf effects is also nearly sufficient to close the SM_d - PDSI gap, perhaps because those effects (Figure 5b) are so consistently positive. That is, the SM_d medlynconst curve in Figure 6 is nearly on top of the PDSI medlynconst curve, except at the lowest percentiles. Thus, CO_2 and VPD physiological effects would combine to much more than account for the SM_d - PDSI response gap in CLM5.0. The main reason that the gap is not quite closed in allelim in spite of this, appears to be the above-discussed negative effects of P temporal pattern change, which widen the gap when eliminated in noflashnoseas (both by increasing SM_d and by decreasing PDSI). The negative nonlinear term (Figure 5f) also likely contributes.

In short, the positive SM_d - PDSI response gap is caused by CO_2 and VPD physiological effects (Figures 5b-c), which increase the SM_d response, and is opposed mainly by P temporal pattern changes (Figures 5d-e), which reduce the SM_d response while in-

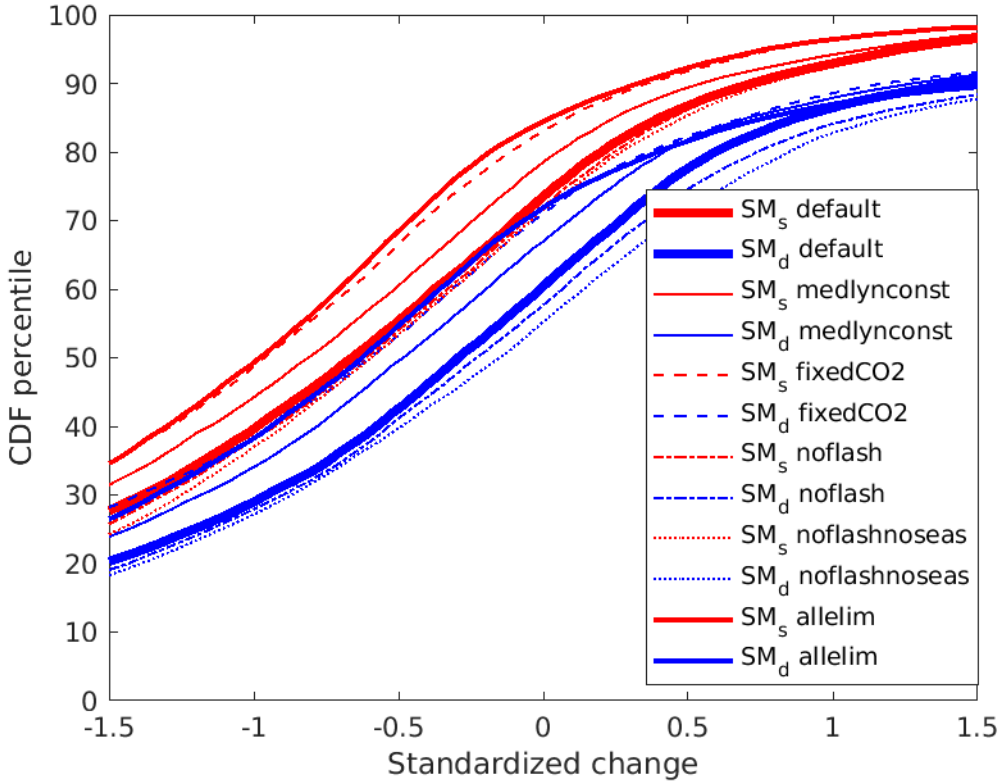

Figure 7. As Figure 3, but for surface soil moisture SM_s (red) and root-zone soil moisture SM_d (blue).

creasing the PDSI response (compare the noflashnoseas and default curves in Figure 6). This is quite different from the Q/P - P/E_0 response gap, which is caused by a combination of all factors as discussed in section 3.1.

3.3 Other gaps

Many other previously noted discrepancies between the responses of different hydroclimate variables are not at all (or only somewhat) reduced in the "allelim" experiment, implying that they are more fundamental. However, in almost all of these cases, there is no theoretical expectation that the responses line up in the first place, unlike for Q/P - P/E_0 or SM_d - PDSI.

For example, Figure 7 shows that the more negative response of surface (SM_s) than root-zone (SM_d) soil moisture found by Berg et al. (2017) is almost completely invariant to the experimental setup, again unlike for Q/P - P/E_0 or SM_d - PDSI above. Similarly, Figure 8 confirms the finding of Scheff et al. (2021) that the apparent relevance of the PDSI for surface LH and SH flux responses (as quantified by the evaporative fraction EF) is just a fortuitous consequence of physiological effects that reduce LH and thus EF (Lemordant et al., 2018). When these are turned off, the EF - PDSI response gap becomes extremely positive.

Figure 9 compares P/E_0 to actual runoff Q rather than runoff ratio Q/P, showing that even in "allelim", Q responds far more positively than P/E_0 (or any of the dry-

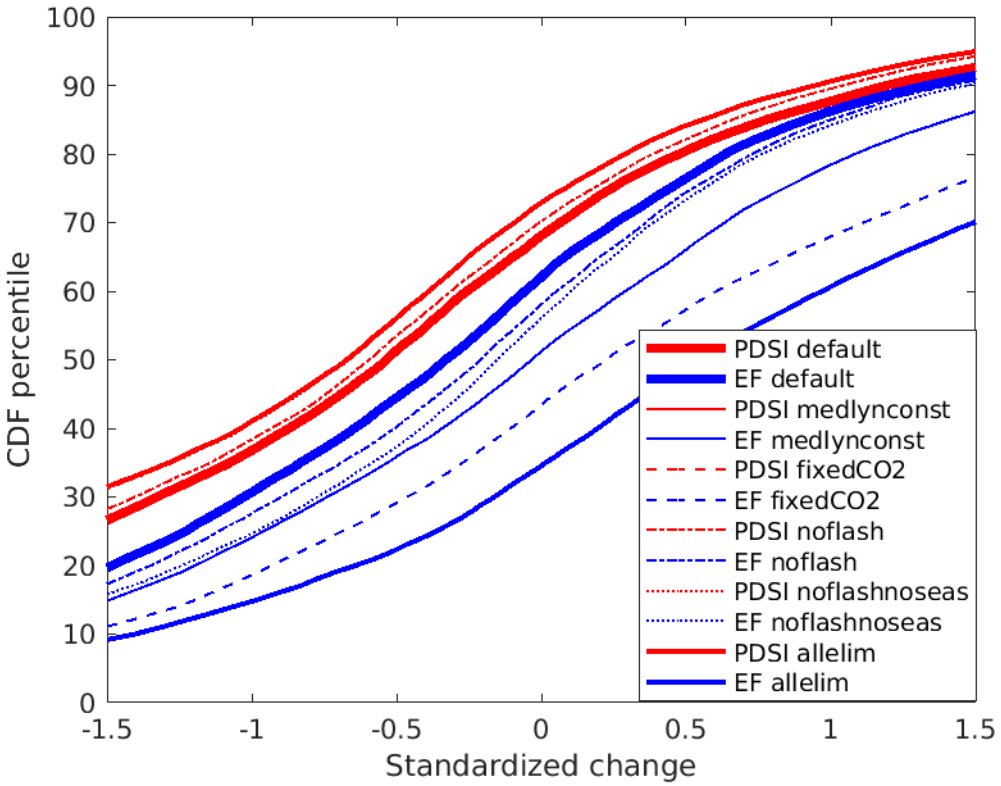

Figure 8. As Figure 3, but for PDSI (red) and evaporative fraction EF (blue).

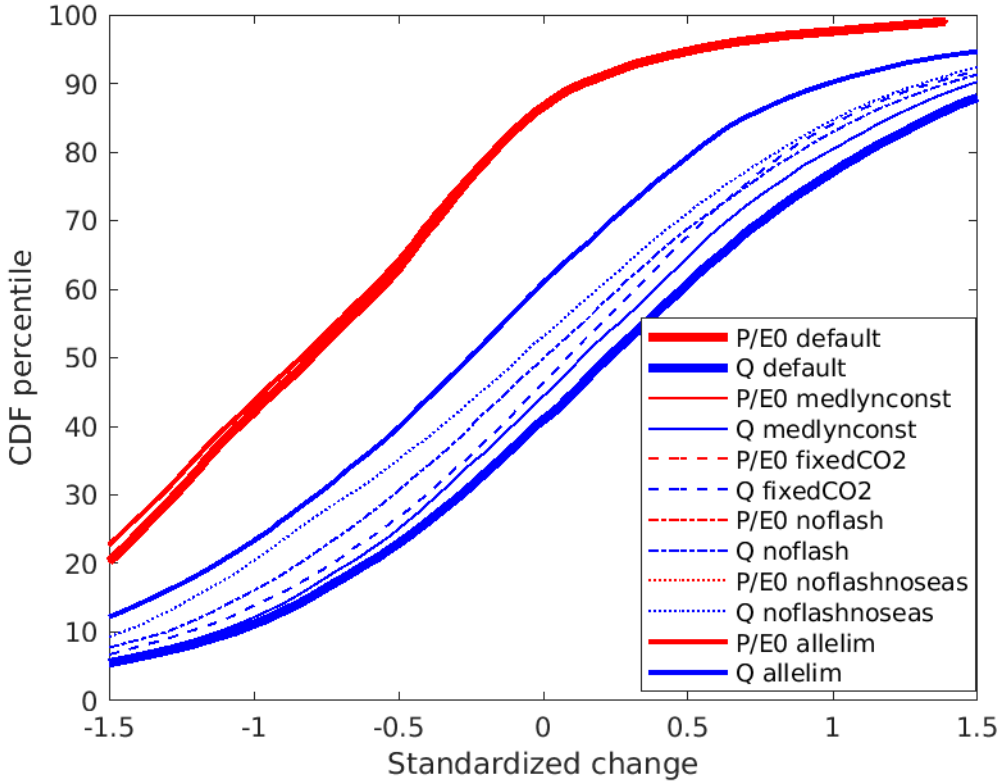

Figure 9. As Figure 3, but for P/E_0 (red) and runoff Q (blue).

ness indices). This is to be expected, since P/E_0 is a predictor of Q/P, but $Q = (Q/P)*P$, and P has a mostly positive response. Finally, Figure 10 shows that even in "allelim", SPEI responds more negatively than SM_d (unlike PDSI, which matches SM_d much more closely as described in section 3.2). This also makes sense, since SPEI (Vicente-Serrano et al., 2010) was not explicitly designed as a SM theory, unlike PDSI.

4 Discussion

On the whole, Figures 1-10 bring much-needed clarity to the multiplicity of contrasting terrestrial hydroclimate responses to greenhouse warming (Seneviratne et al., 2021; Douville et al., 2021), at least in CLM5.0. The simulated Q/P response can be understood as a P/E_0-like, very negative base term (Figure 1d; Q/P allelim curve in Figure 3) plus a series of mostly positive temporal and physiological effects (Figure 2) that cause the full Q/P response to be much less negative (Figure 1c; Q/P default curve in Figure 3). The Q response (Figure 9) can then be understood as a combination of this Q/P response and the largely positive P response, since $Q = (Q/P) * P$.

Similarly, the simulated SM_d response can be understood as a fairly PDSI-like, negative base term (Figure 4d; SM_d allelim curve in Figure 6) plus a series of mostly positive physiological (Figure 5b-c) and negative temporal (Figure 5d-e) effects that in total (Figure 5a) lead to a modest positive enhancement of SM_d compared to PDSI (default curves in Figure 6; Figure 4 (left)). The main reason that the SM_d response is not as positive as the Q/P response seems to be that the P temporal changes, which greatly enhance Q/P, instead act to slightly decrease SM_d.

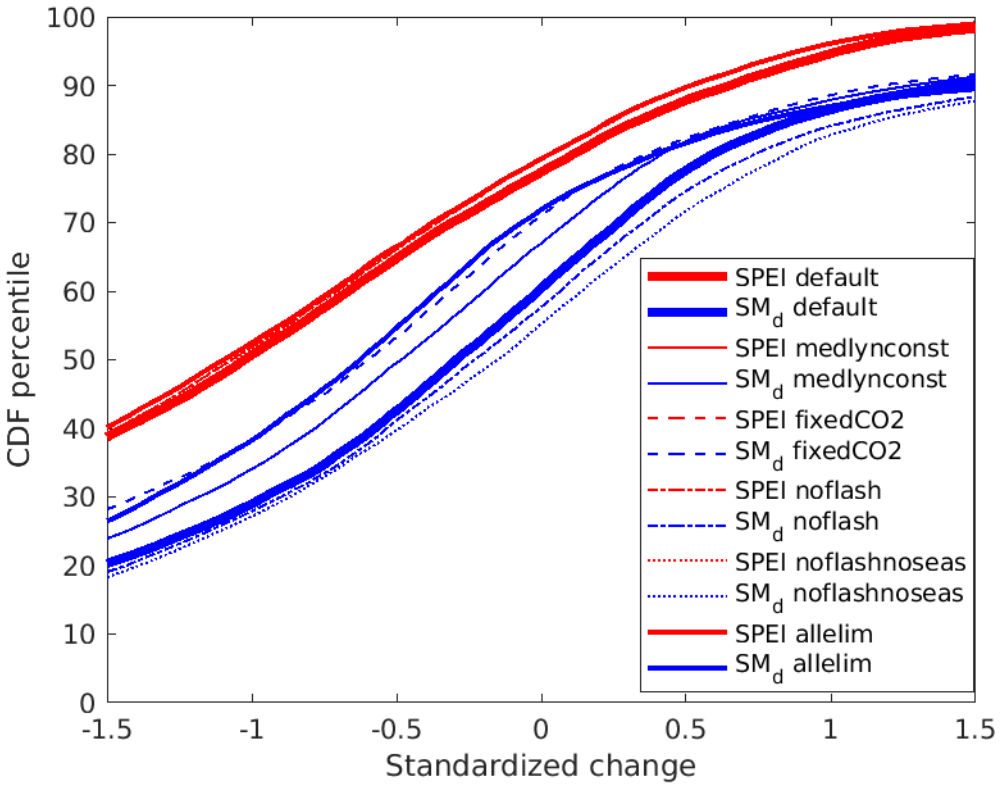

Figure 10. As Figure 3, but for SPEI (red) and SM_d (blue).

The simulated surface-flux (EF) response is also somewhat PDSI-like, but only because of large negative physiological effects (Figure 8). The SPEI response is more negative than the simulated SM_d response in all configurations (Figure 10), in turn making it much more negative than the Q/P or Q responses.

In this way, the long-disputed hydrological meanings of published trends in drought and aridity metrics like P/E_0, PDSI, and SPEI are also clarified. The P/E_0 response to climate change can be interpreted (Figure 1, right) as a model for expected change in Q/P regime sensu Budyko and Miller (1974) *in the absence of P temporal and plant physiological effects*, which at least in CLM5.0 are large. The PDSI response can more tentatively (Figure 4, right) be interpreted as a model for expected SM_d change in the absence of those effects. However, none of the dryness indices can be interpreted as models of expected Q or surface-flux change under any assumptions (Figures 8 and 9). Similarly, the SPEI cannot be interpreted as a model of any expected terrestrial water response to climate change, at least on the basis of CLM5.0's hydrological scheme.

Will the real world behave similarly to CLM5.0? We should perhaps be most confident in the negative "base" (P/E_0- and PDSI-predicted) portions of the Q/P and SM_d responses, since the P/E_0 and PDSI responses themselves are well-understood (e.g., Fu & Feng, 2014; Dai et al., 2018) and their relationships to Q/P and SM_d are long-established (Budyko & Miller, 1974; Palmer, 1965). The plant-physiological and P-temporal effects, by contrast, are not described by such fundamental theories. However, it seems likely that they will all occur to at least some extent (Novick et al., 2016; Mankin et al., 2019; Lemordant et al., 2018; Eekhout et al., 2018), so it would be remiss for us to assume that the real-world SM_d and (especially) Q/P responses will actually be as negative as the PDSI and P/E_0 responses, especially in light of the modeling results presented here.

Further studies should determine whether other land models, and/or fully-coupled models, agree with CLM5.0's simulated physiological and temporal effects on Q/P and SM_d. In planned work, we will also use global observational data to quantify whether real-world long-term trends in Q/P and SM_d are as negative as the P/E_0 and PDSI trends, or whether they more closely resemble full ESM simulations. These investigations will help clarify whether the results of this study are particular to CLM5.0, or more generally applicable.

5 Conclusion

In this study, we carried out a series of experiments with CLM5.0, a widely-used Earth System Model (ESM) land-surface component, to test in a common framework several previously studied or postulated reasons that simulated runoff and soil moisture responses to climate change tend to be more positive than their theorized climatic drivers.

We found that the runoff ratio (Q/P) responds more positively than the aridity index (P/E_0) mainly due to changes in the short-term temporal pattern of P with warming (confirming H. Yang et al., 2018), but also due to changes in P seasonality and the effects of rising CO_2 and vapor pressure deficit (VPD) on plant physiology. The effect of rising CO_2 on plant physiology, in particular, is the key driver of the spatial pattern of the Q/P enhancement.

In contrast, we found that root-zone soil moisture (SM_d) responds somewhat more positively than the Palmer Drought Severity Index (PDSI) mainly due to the above plant-physiological effects (confirming, e.g., Y. Yang et al., 2020), and does so in spite of the P temporal effects, which for SM_d are negative. Runoff itself (Q) responds much more positively than all of these quantities, since $Q = (Q/P) * P$ and the P response tends to be positive. Other key gaps are not well explained by any of the examined processes. Further work will be needed to quantify the broader validity of these results beyond CLM5.0.

6 Open Research

The Community Earth System Model and Community Terrestrial Systems Model (including CLM5.0) source code are publicly available at `https://github.com/ESCOMP/CESM` and `https://github.com/ESCOMP/CTSM`, respectively. The derived monthly and annual hydroclimate variables from each CLM5.0 run in Table 1, as well as all scripts used to set up the runs and process the variables, are archived in Matlab format at Scheff (2022).

References

Allen, R. G., Pereira, L. S., Raes, D., & Smith, M. (1998). *Crop evapotranspiration: guidelines for computing crop water requirements* (Irrigation and Drainage Paper No. 56). Food and Agriculture Organization.

Allen, R. J., & Anderson, R. G. (2018). 21st century California drought risk linked to model fidelity of the El Niño teleconnection. *NPJ Climate and Atmospheric Science*, *1*, 21. doi: 10.1038/s41612-018-0032-x

Berg, A., Findell, K., Lintner, B., Giannini, A., Seneviratne, S. I., B. van den Hurk, ... Milly, P. C. D. (2016). Land-atmosphere feedbacks amplify aridity increase over land under global warming. *Nature Climate Change*, *6*, 869-874. doi: 10.1038/nclimate3029

Berg, A., & Sheffield, J. (2018). Climate change and drought: the soil moisture perspective. *Current Climate Change Reports*, *4*, 180-191. doi: 10.1007/s40641-018-0095-0

Berg, A., Sheffield, J., & Milly, P. C. D. (2017). Divergent surface and total soil moisture projections under global warming. *Geophysical Research Letters*, *44*, 236-244. doi: 10.1002/2016GL071921

Budyko, M. I., & Miller, D. H. (1974). *Climate and life.* Academic Press.

Chou, C., Chiang, J. C. H., Lan, C.-W., Chung, C.-H., Liao, Y.-C., & Lee, C.-J. (2013). Increase in the range between wet and dry season precipitation. *Nature Geoscience*, *6*, 263-267. doi: 10.1038/NGEO1744

Computational and Information Systems Laboratory. (2019). *Cheyenne: HPE/SGI ICE XA System (University Community Computing).* Boulder, CO: National Center for Atmospheric Research. doi: 10.5065/D6RX99HX

Cook, B. I., Mankin, J. S., Marvel, K., Williams, A. P., Smerdon, J. E., & Anchukaitis, K. J. (2020). Twenty-first century drought projections in the CMIP6 forcing scenarios. *Earth's Future*, *8*, e2019EF001461. doi: 10.1029/2019EF001461

Dai, A., Zhao, T., & Chen, J. (2018). Climate change and drought: a precipitation and evaporation perspective. *Current Climate Change Reports*, *4*, 301-312. doi: 10.1007/s40641-018-0101-6

Danabasoglu, G., Lamarque, J.-F., Bacmeister, J., Bailey, D. A., DuVivier, A. K., Edwards, J., ... Strand, W. G. (2020). The Community Earth System Model version 2 (CESM2). *Journal of Advances in Modeling Earth Systems*, *12*, e2019MS001916. doi: 10.1029/2019MS001916

Douville, H., Raghavan, K., Renwick, J., Allan, R. P., Arias, P. A., Barlow, M., ... Zolina, O. (2021). Water cycle changes. In V. Masson-Delmotte et al. (Eds.), *Climate Change 2021: The Physical Science Basis. Contribution of Working Group I to the Sixth Assessment Report of the Intergovernmental Panel on Climate Change.* Cambridge University Press.

Eekhout, J. P. C., Hunink, J. E., Terink, W., & de Vente, J. (2018). Why increased extreme precipitation under climate change negatively affects water security. *Hydrology and Earth System Science*, *22*, 5935-5946. doi: 10.5194/hess-22-5935-2018

Eyring, V., Bony, S., Meehl, G. A., Senior, C. A., Stevens, B., Stouffer, R. J., &

Taylor, K. E. (2016). Overview of the Coupled Model Intercomparison Project Phase 6 (CMIP6) experimental design and organization. *Geoscientific Model Development*, *9*, 1937-1958. doi: 10.5194/gmd-9-1937-2016

Fu, Q., & Feng, S. (2014). Responses of terrestrial aridity to global warming. *Journal of Geophysical Research*, *119*, 7863-7875. doi: 10.1002/2014JD021608

Gentine, P., D'Odorico, P., Lintner, B. R., Sivandran, G., & Salvucci, G. (2012). Interdependence of climate, soil, and vegetation as constrained by the Budyko curve. *Geophysical Research Letters*, *39*, L19404. doi: 10.1029/2012GL053492

Greve, P., Roderick, M. L., Ukkola, A. M., & Wada, Y. (2019). The aridity index under global warming. *Environmental Research Letters*, *14*, 124006. doi: 10.1088/1748-9326/ab5046

Jones, C. D., Arora, V., Friedlingstein, P., Bopp, L., Brovkin, V., Dunne, J., ... Zaehle, S. (2016). C4MIP - The Coupled Climate-Carbon Cycle Model Intercomparison Project: experimental protocol for CMIP6. *Geoscientific Model Development*, *9*, 2853-2880. doi: 10.5194/gmd-9-2853-2016

Kim, D., Sobel, A. H., & Kang, I.-S. (2011). A mechanism denial study on the Madden-Julian Oscillation. *Journal of Advances in Modeling Earth Systems*, *3*, M12007. doi: 10.1029/2011MS000081

Lawrence, D. M., Fisher, R. A., Koven, C. D., Oleson, K. W., Swenson, S. C., Bonan, G., ... Zeng, X. (2019). The Community Land Model version 5: Description of new features, benchmarking, and impact of forcing uncertainty. *Journal of Advances in Modeling Earth Systems*, *11*, 4245-4287. doi: 10.1029/2018MS001583

Lee, J.-Y., Marotzke, J., Bala, G., Cao, L., Corti, S., Dunne, J. P., ... Zhou, T. (2021). Future global climate: scenario-based projections and near-term information. In V. Masson-Delmotte et al. (Eds.), *Climate Change 2021: The Physical Science Basis. Contribution of Working Group I to the Sixth Assessment Report of the Intergovernmental Panel on Climate Change.* Cambridge University Press.

Lemordant, L., Gentine, P., Swann, A. S., Cook, B. I., & Scheff, J. (2018). Critical impact of vegetation physiology on the continental hydrologic cycle in response to increasing CO_2. *Proceedings of the National Academy of Sciences of the USA*, *115*, 4093-4098. doi: 10.1073/pnas.1720712115

Mankin, J. S., Seager, R., Smerdon, J. E., Cook, B. I., & Williams, A. P. (2019). Mid-latitude freshwater availability reduced by projected vegetation responses to climate change. *Nature Geoscience*, *12*, 983-988. doi: 10.1038/s41561-019-0480-x

Mankin, J. S., Seager, R., Smerdon, J. E., Cook, B. I., Williams, A. P., & Horton, R. M. (2018). Blue water trade-offs with vegetation in a CO_2-enriched climate. *Geophysical Research Letters*, *45*, 3115-3125. doi: 10.1002/2018GL077051

Massmann, A., Gentine, P., & Lin, C. (2019). When does vapor pressure deficit drive or reduce evapotranspiration? *Journal of Advances in Modeling Earth Systems*, *11*, 3305-3320. doi: 10.1029/2019MS001790

Medlyn, B. E., Duursma, R. A., Eamus, D., Ellsworth, D. S., Prentice, I. C., Barton, C. V. M., ... Wingate, L. (2011). Reconciling the optimal and empirical approaches to modelling stomatal conductance. *Global Change Biology*, *17*, 2134-2144. doi: 10.1111/j.1365-2486.2010.02375.x

Milly, P. C. D., & Dunne, K. A. (2016). Potential evapotranspiration and continental drying. *Nature Climate Change*, *6*, 946-949. doi: 10.1038/nclimate3046

Milly, P. C. D., & Dunne, K. A. (2017). A hydrologic drying bias in water-resource impact analyses of anthropogenic climate change. *Journal of the American Water Resources Association*, *53*, 822-838. doi: 10.1111/1752-1688.12538

Naumann, G., Alfieri, L., Wyser, K., Mentaschi, L., Betts, R. A., Carrao, H., ... Feyen, L. (2018). Global changes in drought conditions under different levels of warming. *Geophysical Research Letters*, *45*, 3285-3296. doi:

10.1002/2017GL076521

Novick, K. A., Ficklin, D. L., Stoy, P. C., Williams, C. A., Bohrer, G., Oishi, A. C., ... Phillips, R. P. (2016). The increasing importance of atmospheric demand for ecosystem water and carbon fluxes. *Nature Climate Change*, *6*, 1023-1027. doi: 10.1038/NCLIMATE3114

Palmer, W. C. (1965). *Meteorological drought* (Research Paper No. 45). U.S. Weather Bureau.

Pendergrass, A. G., & Hartmann, D. L. (2014). Changes in the distribution of rain frequency and intensity in response to global warming. *Journal of Climate*, *27*, 8372-8383. doi: 10.1175/JCLI-D-14-00183.1

Qi, Y., Yu, H., Fu, Q., Chen, Q., Ran, J., & Yang, Z. (2022). Future changes in drought frequency due to changes in the mean and shape of the PDSI probability density function under RCP4.5 scenario. *Frontiers in Earth Science*, *10*, 857885. doi: 10.3389/feart.2022.857885

Roderick, M. L., Greve, P., & Farquhar, G. D. (2015). On the assessment of aridity with changes in atmospheric CO2. *Water Resources Research*, *51*, 5450-5463. doi: 10.1002/2015WR017031

Scheff, J. (2018). Drought indices, drought impacts, CO_2, and warming: a historical and geologic perspective. *Current Climate Change Reports*, *4*, 202-209. doi: 10.1007/s40641-018-0094-1

Scheff, J. (2022). *Replication Data for: Why do the Global Warming Responses of Land-surface Models and Climatic Dryness Metrics Disagree? [Dataset and Software].* UNC Dataverse. doi: 10.15139/S3/AENJTV

Scheff, J., Mankin, J. S., Coats, S., & Liu, H. (2021). CO2-plant effects do not account for the gap between dryness indices and projected dryness impacts in CMIP6 or CMIP5. *Environmental Research Letters*, *16*, 034018. doi: 10.1088/1748-9326/abd8fd

Scheff, J., Seager, R., Liu, H., & Coats, S. (2017). Are glacials dry? Consequences for paleoclimatology and for greenhouse warming. *Journal of Climate*, *30*, 6593-6609. doi: 10.1175/JCLI-D-16-0854.1

Seneviratne, S. I., Zhang, X., Adnan, M., Badi, W., Dereczynski, C., Luca, A. D., ... Zhou, B. (2021). Weather and climate extreme events in a changing climate. In V. Masson-Delmotte et al. (Eds.), *Climate Change 2021: The Physical Science Basis. Contribution of Working Group I to the Sixth Assessment Report of the Intergovernmental Panel on Climate Change.* Cambridge University Press.

Swann, A. L. S., Hoffman, F. M., Koven, C. D., & Randerson, J. T. (2016). Plant responses to increasing CO2 reduce estimates of climate impacts on drought severity. *Proceedings of the National Academy of Sciences of the USA*, *113*, 10019-10024. doi: 10.1073/pnas.1604581113

Transeau, E. N. (1905). Forest centers of eastern America. *Amer. Naturalist*, *39*, 875-889.

Vicente-Serrano, S. M., Beguería, S., & López-Moreno, J. I. (2010). A multiscalar drought index sensitive to global warming: the standardized precipitation evapotranspiration index. *Journal of Climate*, *23*, 1696-1718. doi: 10.1175/2009JCLI2909.1

Vicente-Serrano, S. M., Domínguez-Castro, F., McVicar, T. R., Tomas-Burguera, M., Peña-Gallardo, M., Noguera, I., ... Kenawy, A. E. (2020). Global characterization of hydrological and meteorological droughts under future climate change: The importance of timescales, vegetation-CO2 feedbacks and changes to distribution functions. *International Journal of Climatology*, *40*, 2557-2567. doi: 10.1002/joc.6350

Wang, X., Jiang, D., & Lang, X. (2020). Future changes in Aridity Index at two and four degrees of global warming above preindustrial levels. *International Journal of Climatology*. doi: 10.1002/joc.6620

Yang, H., Piao, S., Huntingford, C., Ciais, P., Li, Y., Wang, T., ... Chang, J. (2018). Changing the retention properties of catchments and their influence on runoff under climate change. *Environmental Research Letters*, *13*, 094019. doi: 10.1088/1748-9326/aadd32

Yang, Y., Roderick, M. L., Zhang, S., McVicar, T. R., & Donohue, R. J. (2019). Hydrologic implications of vegetation response to elevated CO_2 in climate projections. *Nature Climate Change*, *9*, 44-48. doi: 10.1038/s41558-018-0361-0

Yang, Y., Zhang, S., Roderick, M. L., McVicar, T. R., Yang, D., Liu, W., & Li, X. (2020). Comparing PDSI drought assessments using the traditional offline approach with direct climate model outputs. *Hydrology and Earth System Science*, *24*, 2921-2930. doi: 10.5194/hess-24-2921-2020

Zhao, T., & Dai, A. (2015). The magnitude and causes of global drought changes in the twenty-first century under a low-moderate emissions scenario. *Journal of Climate*, *28*, 4490-4512. doi: 10.1175/JCLI-D-14-00363.1

Zhou, S., Williams, A. P., Lintner, B. R., Berg, A. M., Zhang, Y., Keenan, T. F., ... Gentine, P. (2021). Soil moisture-atmosphere feedbacks mitigate declining water availability in drylands. *Nature Climate Change*, *11*, 38-44. doi: 10.1038/s41558-020-00945-z